Acta Cryst B
STRUCTURAL SCIENCE
CRYSTAL ENGINEERING
MATERIALS
ISSN 2052-5206

Variations of quantum electronic pressure under the external compression in crystals with halogen bonds assembled in Cl_3-, Br_3-, I_3-synthons

Ekaterina Bartashevich,[a]* Sergey Sobalev,[a] Yury Matveychuk[a] and Vladimir Tsirelson[a,b]

[a]Research Laboratory of Multiscale Modelling of Functional Materials, South Ural State University, 76, Lenin ave., Chelyabinsk, 454080, Russian Federation, and [b]Quantum Chemistry Department, Dmitry Mendeleev University of Chemical Technology of Russia, 9, Miusskaya sq., Moscow, 125047, Russian Federation. *Correspondence e-mail: bartashevichev@susu.ru

Received 4 March 2020
Accepted 5 May 2020

Edited by A. Katrusiak, Adam Mickiewicz University, Poland

Keywords: quantum electronic pressure; Hal_3-synthon; halogen bond; external compression; electron density.

Supporting information: this article has supporting information at journals.iucr.org/b

The inner-crystal quantum electronic pressure was estimated for unstrained C_6Cl_6, C_6Br_6, and C_6I_6 crystals and for those under external compression simulated from 1 to 20 GPa. The changes in its distribution were analyzed for the main structural elements in considered crystals: for triangles of the typical halogen bonds assembled in Hal_3-synthons, where Hal = Cl, Br, I; for Hal···Hal stacking interactions, as well as for covalent bonds. Under simulated external compression, the quantum electronic pressure in the intermolecular space reduces as the electron density increases, indicating spatial areas of relatively less crystal resistance to external compression. The most compliant C_6Cl_6 crystal shows the largest changes of quantum electronic pressure in the centre of Cl_3-synthon while the deformation of rigid I_3-synthon under external compression depends only on the features of I···I halogen bonds.

1. Introduction

Characterization and prediction of mechanical properties, such as stiffness, brittleness, elasticity or plasticity of crystal structures, are directly related to the changes at the level of noncovalent interactions (Coudert & Fuchs, 2016; Mishra *et al.*, 2020; Feng *et al.*, 2016). Research of bonding effects in molecular crystals in ambient conditions and under external stress has been performed in both experimental studies (Bag *et al.*, 2012; Casati *et al.*, 2017; Mishra *et al.*, 2017; Saha *et al.*, 2018; Arkhipov *et al.*, 2019) and those using density functional theory (DFT) calculations (Lin *et al.*, 2017; Matveychuk *et al.*, 2018; Colmenero, 2019*a*,*b*; Giordano *et al.*, 2019). The popular targets in the investigation of mechanical properties were the hexahalobenzene molecular crystals, C_6Cl_6, C_6Br_6 and C_6I_6, including their treatment under external compression. Changes in crystalline structure and conductivity of C_6I_6 were studied both experimentally (Iwasaki *et al.*, 2001; Nakayama *et al.*, 2000, 2001; Shirotani *et al.*, 1976) and theoretically (Tateyama & Ohno, 2002). For the hexaiodobenzene crystal, the metallization was noted at 35 GPa and the superconductivity in metal phase was observed at 2 K (Iwasaki *et al.*, 2001). X-ray powder diffraction perfomed on a crystal under compression up to 9.7 GPa showed a monoclinic structure with significant decrease in the *b* axis (Nakayama *et al.*, 2000). The intermolecular I···I interactions were located in the *bc* plane. The C_6I_6 crystal was analyzed using Raman spectroscopy at compression up to 47 GPa (Nakayama *et al.*,

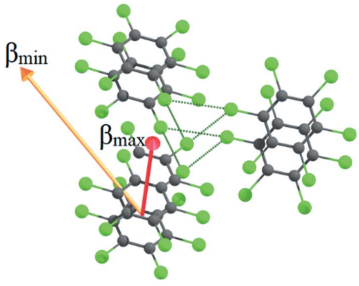

2001) and its resistivity up to 50 GPa was studied (Shirotani *et al.*, 1976). The compressibility of the C_6Cl_6 and C_6Br_6 crystals under compression up to 4.5 GPa was also examined (Vaidya & Kennedy, 1971). The high-pressure X-ray diffraction and Raman spectra measurements were carried out for the C_6F_6 crystals up to 1.9 GPa (Rusek *et al.*, 2020) and at 34.4 GPa (Pravica *et al.*, 2016).

For the halogenated molecules in crystals, the characteristic structural motif is known, consisting of three halogen bonds joined in a common ring, called a Hal_3-synthon (Reddy *et al.*, 2006; Bui *et al.*, 2009). Also, they can form hetero-halogen-bonded trimers with different types of noncovalent interactions (Pavan & Guru Row, 2016). For Hal_3-synthons both the electrophilic and nucleophilic sites of halogen atoms are involved in halogen bonding, where the σ-hole (Clark *et al.*, 2007; Politzer & Murray, 2019) of one halogen atom is directed to the equatorial electronic belt of the neighbouring one. As a result, each halogen atom simultaneously provides both electrophilic and nucleophilic sites during the formation of a halogen bond (Saha *et al.*, 2005; Hathwar & Guru Row, 2010). The ability of Hal_3-synthons to increase the strength and mutual influence of Hal$\cdots$Hal interactions was pointed out by Desiraju & Pathasarathy (1989). It was established that Hal_3-synthons could be effectively used in the design of host frameworks (Jetti *et al.*, 1999; Saha *et al.*, 2005), as well as in crystal engineering (Bosch & Barnes, 2002; Brezgunova *et al.*, 2012). Further analysis confirmed the anisotropic charge density distribution around the halogen atoms. In addition, Saha *et al.* (2005) found that in Br_3-synthons the interactions between the positively and negatively charged regions were stronger than in Cl_3-synthons. It was noted that the phase with F_3-synthon in C_6F_6 could exist in a very narrow pressure range (Pravica *et al.*, 2016). The F$\cdots$F halogen bonds are much less common; nevertheless, for substituted perfluorobenzenes, they have been carefully analyzed by X-ray diffraction (Siram *et al.*, 2013; Pavan *et al.*, 2013; Moussallem *et al.*, 2015).

The features of noncovalent interactions such as the halogen (Desiraju *et al.*, 2013), chalcogen, pnictogen or tetrel bonds (Aakeroy *et al.*, 2019) influence a number of properties of molecular crystals, including their response to external compression. Understanding the nature of electrostatically driven noncovalent bonds is directly linked to an idea of anisotropy of electronic features of outer atomic electron shells. For example, the electrostatic potential indicates the electrophilic and nucleophilic sites that can be provided by the covalently bound atoms for the possible noncovalent bonding (Murray & Politzer, 2011; Politzer & Murray, 2019). Descriptors for chemical bonds and noncovalent interactions that are based on electron density and its derivatives and integrals make it possible to evaluate the anisotropy of atomic electron distribution and its effect on the structural features of molecular crystals (Tsirelson & Ozerov, 1996). The simplest tool that very clearly demonstrated the electronic features of a typical halogen bond in the Cl_2 crystal is the Laplacian of electron density (Tsirelson *et al.*, 1995). The electron accumulation of one chlorine atom faces the electron depletion in a chlorine atom of a neighbouring molecule. Also, the one-electron potential (Hunter, 1986) was proposed as a promising tool for the description of iodine–iodine halogen bonds in crystals with polyiodide chains (Bartashevich *et al.*, 2014, 2017). While the classical electrostatic potential illustrates the predisposition of a halogenated molecule to the halogen bond formation, by virtue of including an exchange contribution, the potential acting on an electron in a molecule (PAEM) (Yang & Davidson, 1997; Zhao & Yang, 2014) can be successfully applied for more detailed characterization of noncovalent bonds (Bartashevich & Tsirelson, 2018).

Tao *et al.* (2008) and Tsirelson *et al.* (2019) have indicated that the quantum internal pressure of inhomogeneous electron continuum in the nuclei field reflects the space electron concentrations and depletions in molecules and crystals. Internal pressure describes the variations in the average internal energy of a unit volume of the electron continuum under the local deformation that changes the volume without changing its shape (Tsirelson *et al.*, 2016). The kinetic contribution to the quantum electronic pressure, QEP(**r**), can be expressed via the electron continuum stress tensor (Bader, 1990); the exchange-correlation contribution can be expressed via DFT functionals (Becke, 1988). The effect of electron correlation is significantly weaker than exchange contribution (Tsirelson *et al.*, 2019), and it may be neglected in the first approximation. As a result, the function QEP(**r**) is defined in a simple form:

$$\mathrm{QEP}(\mathbf{r}) = \frac{2}{3}g(\mathbf{r}) - \frac{1}{4}\nabla^2\rho(\mathbf{r}) - \frac{1}{4}\left(\frac{3}{\pi}\right)^{\frac{1}{3}}\rho(\mathbf{r})^{4/3}. \qquad (1)$$

Here, the first two terms describe the kinetic contribution, where $g(\mathbf{r})$ is the positively defined kinetic energy density of electrons. It can be calculated directly from the wavefunction or can be obtained in DFT on the basis of Kirzhnits-like approximations (Astakhov *et al.*, 2016). The third term is the exchange contribution to the quantum electronic pressure in the local density approximation (Tao *et al.*, 2008). The QEP(**r**) describes the distribution of the quantum part of electron energy in the field of electrons and nuclei, not the actual density of electrons. For covalent bonds QEP(**r**) > 0, this means that the crystal compression increases the internal electronic energy in such regions. For noncovalent interactions QEP(**r**) < 0, as a rule. Since the external hydrostatic pressure mainly pushes molecules to each other, the changes in the electron continuum of intermolecular space are the most sensitive to variation in mechanical properties. They indicate the areas in which the quantum contribution to the local internal energy of electron continuum must get low to compensate the stress growing under the external compression. Thus, QEP(**r**) can locally increase or decrease, depending on the nature of external deformation.

Our study models. for the first time, the variations in the internal quantum electronic pressure, QEP(**r**), in Hal_3-synthons under external compression. The focus of our attention has been directed at hexachlorobenzene (HCLBNZ13) (Bui *et al.*, 2009), hexabromobenzene (HBRBEN03) (Brezgunova *et al.*, 2012) and hexaiodobenzene

Table 1
The changes in the absolute values and relative percentage changes of quantum electronic pressure and electron density at bond critical point (bcp) and ring critical point (rcp) (a.u.) in the C_6Hal_6 crystals under external compression from 0 to 20 GPa.

The averaged data for three Hal···Hal halogen bonds of a Hal_3-synthon are shown.

Bond or ring critical point	$\Delta\rho(\mathbf{r})$ (a.u.)	$\Delta\rho(\mathbf{r})$ %	ΔQEP($\mathbf{r}$) (a.u.)	ΔQEP($\mathbf{r}$) %
C_6Cl_6				
Covalent C—Cl, bcp	0.016	7.5	0.018	18.9
Covalent C—C, bcp	0.011	3.5	0.017	7.7
Halogen bond Cl···Cl, bcp	0.018	373.8	0.007	256.6
Stacking interaction Cl···Cl, bcp	0.012	231.3	0.005	216.4
Cl_3-synthon, rcp	0.010	477.3	0.006	504.8
Benzene ring C_6, rcp	0.002	10.9	0.002	10.1
C_6Br_6				
Covalent C—Br, bcp	0.014	8.5	0.011	18.3
Covalent C—C, bcp	0.012	3.8	0.019	8.6
Halogen bond Br···Br, bcp	0.019	317.1	0.005	187.0
Stacking interaction Br···Br, bcp	0.014	258.3	0.004	160.0
Br_3-synthon, rcp	0.011	403.0	0.005	331.4
Benzene ring C_6, rcp	0.002	12.4	0.002	11.6
C_6I_6				
Covalent C—I, bcp	0.013	11.0	0.007	29.4
Covalent C—C, bcp	0.014	4.7	0.022	10.5
Halogen bond I···I, bcp	0.020	195.0	0.002	57.3
Stacking interaction I···I, bcp	0.015	216.5	0.002	109.7
I_3-synthon, rcp	0.012	244.0	0.003	168.2
Benzene ring C_6, rcp	0.003	15.0	0.003	14.4

(HIBENZ11) (Ghosh *et al.*, 2007) crystals. Among all possible crystal structures in the Cambridge Structural Database (Groom *et al.*, 2016), we have selected those refined with the lowest *R*-factor. These crystals are isostructural, the first half of the hexahalobenzene molecule belongs to the asymmetric unit, and the second one is generated by the inversion centre located inside the benzene ring. We consider and compare the distributions of the quantum electronic pressure for the Hal···Hal halogen bonds and Hal···Hal stacking interaction, the covalent C—Hal and C—C bonds, as well as the centres of Hal_3-synthons and benzene rings. It is important that our analysis of electronic properties for different types of bonding has been performed under external compression of 1, 5, 10 and 20 GPa simulated in the stage of geometry optimization.

2. Calculations

The geometrical parameters of the C_6Cl_6, C_6Br_6 and C_6I_6 crystal structures were optimized under the conditions of external compression when the Hellmann–Feynman forces were equal to zero (Feynman, 1939). The Kohn–Sham method (Koch & Holthausen, 2001) and *CRYSTAL17* program (Dovesi *et al.*, 2018) were used. Calculations were carried out using basis sets 6-31G(d) (Francl *et al.*, 1982) for the C atoms and DZVP (Godbout *et al.*, 1992) for the Hal atoms taking into account the Grimme dispersion correction D3 (Grimme *et al.*, 2010).

Since the electron density for the hexachlorobenzene crystal, obtained from high-precision X-ray diffraction data, was known due to the work of Bui *et al.* (2009), we used these data for the DFT method selection. We examined HSE06, PBE0 and B3LYP functionals for localization of equilibrium states of the C_6Cl_6 crystal. Atomic positions and unit-cell parameters were optimized. The root-mean-square (r.m.s.) deviations from experimental data comprise 0.031 Å, 0.033 Å, 0.083 Å for above-mentioned functionals, respectively. Note that the HSE06/6-31G(d)/DZVP level with Grimme D3 correction led to the relatively small r.m.s. deviations for calculated atomic coordinates after full optimization of crystallographic cells for C_6Br_6 (0.036 Å) and for C_6I_6 (0.053 Å). Therefore, we used the exchange-correlation functional HSE06 (Perdew *et al.*, 1996) in all subsequent calculations in this study.

Distortion of crystal structures under the external compression was simulated with complete relaxation of atomic coordinates and unit-cell parameters, see Table S1. The following convergence parameters were used for all calculations: TOLDEG (r.m.s. on gradient) was less than 0.00001 a.u., TOLDEX (r.m.s. on estimated displacement) was less than 0.00003 a.u., TOLDEE (energy change between optimization steps threshold) was less than 10^{-10} a.u., TOLINTEG (truncation criteria for bi-electronic integrals) were 14 14 14 14 24. The SHRINK parameter, which determines the number of *k*-points in the reciprocal space in the Pack–Monkhorst scheme, at which the Kohn–Sham matrix was diagonalized, was set to 8 16. In addition, the stiffness tensors of the C_6Cl_6, C_6Br_6 and C_6I_6 crystals were calculated with the ELASTCON (Perger *et al.*, 2009) option for unstrained crystal structures and for structures under external compression. The Hill bulk moduli were estimated and the spatial dependences of elastic moduli were obtained using *ELATE* online tool (Gaillac *et al.*, 2016; Gaillac & Coudert, 2016). Since the spatial dependences of linear compressibility were determined in polar coordinates, the Cartesian coordinates were recalculated into polar ones

for the required direction and the points on the surface of spatial dependences were determined as they carry information about compressibility in such a direction. As an alternative method for bulk moduli estimation, we used the PASCal online tool (Cliffe & Goodwin, 2012).

For the estimation of quantum electronic pressure [QEP(**r**), equation (1)] the distributions of electron density [$\rho(\mathbf{r})$], Laplacian of electron density [$\nabla^2\rho(\mathbf{r})$] and the electronic kinetic energy density [$g(\mathbf{r})$] were calculated for crystals in optimal equilibrium geometries. Quantum topological analysis (Bader, 1990, 1991) of the calculated electron density, based on the *CRYSTAL17* wavefunctions, was performed using *TOPOND* program (Gatti, 1996; Gatti & Casassa, 2016). For all considered C_6Cl_6, C_6Br_6 and C_6I_6 crystals, the values of quantum electronic pressure at the bond critical points (bcp) and ring critical points (rcp) of electron density (Bader, 1990, 1991) were analyzed by modelling the external compression at 1, 5, 10 and 20 GPa. We estimated the percentage changes in the values of electron density [$\Delta\rho(\mathbf{r})$] and quantum electronic pressure [ΔQEP(**r**)] (see Table 1) as follows. Firstly, we found the difference in the $\rho(\mathbf{r})$ or QEP(**r**) values at 0 GPa and at 20 GPa. Secondly, we reduced these differences to the values observed without external compression.

An alternative way of QEP(**r**) estimation used the experimental electron density for the C_6Cl_6 crystal (Bui *et al.*, 2009). It was realized from the *WinXPRO 3.4.11* program (Stash & Tsirelson, 2002; Stash & Tsirelson, 2005; Stash & Tsirelson, 2014). The electron density and its derivatives were expressed in terms of Hansen and Coppens (1978) multipole model and atomic electronic wavefunctions by Macchi & Coppens (2001). The kinetic energy density of electrons was calculated in Kirzhnits (1957) approximation and the exchange contribution to the quantum electronic pressure was obtained using the local Dirac exchange potential.

All calculations with periodic boundary conditions were performed on the TORNADO supercomputer of South Ural State University (Kostenetskiy & Semenikhina, 2018).

3. Results and discussion

Comparison of experimental and equilibrium geometry of the hexahalobenzene crystals showed that the halogen bonds in the non-equilateral triangle of Hal_3-synthon (Fig. 1) retained their proportions which did not greatly change even in compressed crystals. The calculated distances of the Cl···Cl and Br···Br halogen bonds are longer than the experimental values by 0.034 Å, on average, while the I···I halogen bond is shorter by 0.040 Å. The C—Hal covalent bond lengths are longer than the experimental values by 0.009 Å, on average. With an increase in external compression, a decrease in distances of both the halogen and covalent bonds is observed in all crystals. Among the considered crystals, the largest shortening of the halogen bond occurs in C_6Cl_6 and the smallest one is in C_6I_6. For covalent bonds, the situation is opposite: the largest relative shortening is in the C_6I_6 crystal (Table S2).

If we compare the electron density, $\rho(\mathbf{r})$, calculated in the present study using DFT wavefunctions, and the experimentally obtained $\rho(\mathbf{r})$ function (Bui *et al.*, 2009), we shall see that for the C_6Cl_6 crystal the calculated values at bcp are not much smaller than the experimental data (Table S2). With increasing external compression, the electron density at bcp of halogen bonds and Hal···Hal stacking interactions does not grow linearly, but the tendencies are similar; for the halogen bonds the values of $\rho(\mathbf{r}_{bcp})$ are greater than those for stacking interactions. The differences for the values of electron density and quantum electronic pressure in two extreme points of simulated compression, namely, 0 and 20 GPa, are listed in Table 1. It is interesting to note that the electron density enlargement under the external compression which changes from 0 up to 20 GPa, on average, is the same for all types of bonds; it is $\Delta\rho(\mathbf{r}_{bcp}) = 0.016\pm0.004$ a.u. Nevertheless, the pattern of relative electron density increasing under compression looks different: for noncovalent bonds and intermolecular continuum the relative percentage change of $\rho(\mathbf{r}_{bcp})$ is two orders higher than for covalent bonds. In general, the relative percentage change of electron density for the C—Hal covalent bonds increases in order: C—Cl < C—Br < C—I, and for the Hal···Hal halogen bonds it falls in order: Cl···Cl > Br···Br > I···I. The absolute values of $\Delta\rho(\mathbf{r}_{rcp})$ for Hal_3-synthons are smaller, on average, than $\Delta\rho(\mathbf{r}_{bcp})$ for halogen bonds. However, the percentage values of the change in electron density are quite large: 244.0% for I_3-synthon and 477.3% for Cl_3-synthon. The values of electron density at rcp of benzene rings are always higher; however, their changes under compression, $\Delta\rho(\mathbf{r}_{rcp})$, are much smaller and do not exceed 15% for all considered crystals. Thus, the largest changes in electron density under compression are inherent for the C_6Cl_6 crystal.

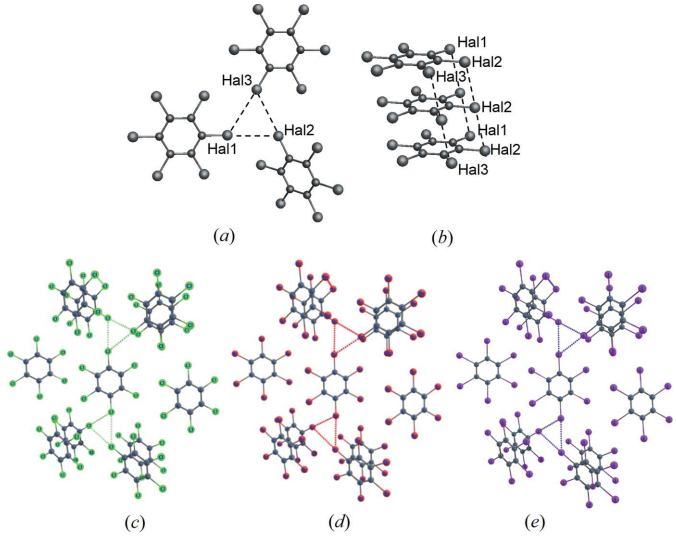

Figure 1
(*a*) Hal_3-synthon and (*b*) Hal···Hal stacking interactions (Hal = Cl, Br, I) in isostructural crystals: (*c*) C_6Cl_6, (*d*) C_6Br_6, and (*e*) C_6I_6.

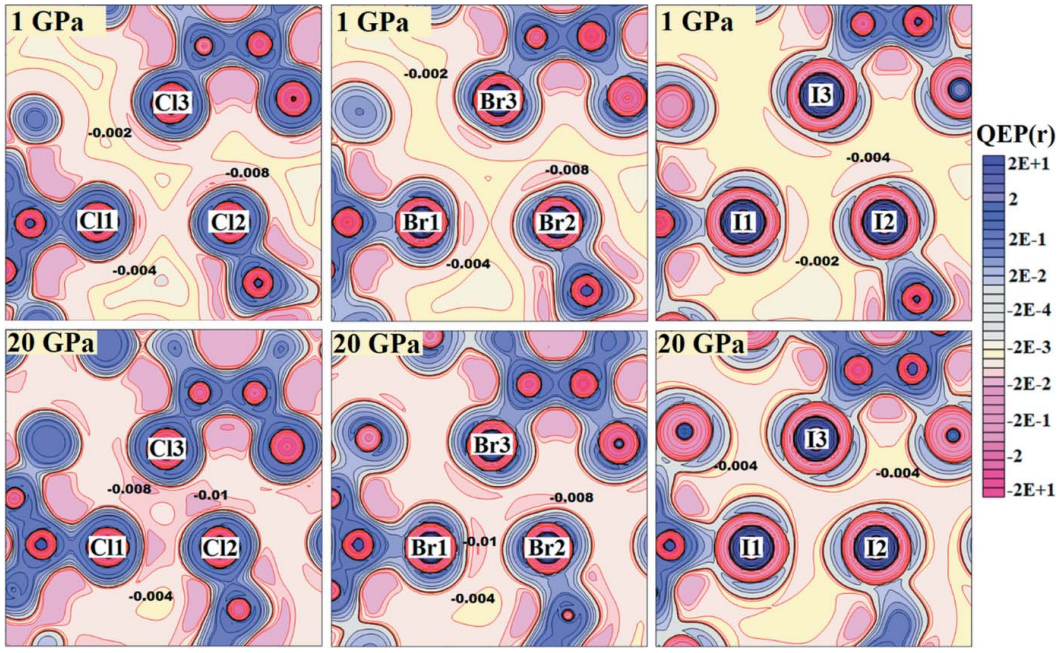

Figure 2
Maps of quantum electronic pressure for (*a*) Cl_3-synthons, (*b*) Br_3-synthons, (*c*) I_3-synthons under compression of 1 GPa (top) and 20 GPa (bottom).

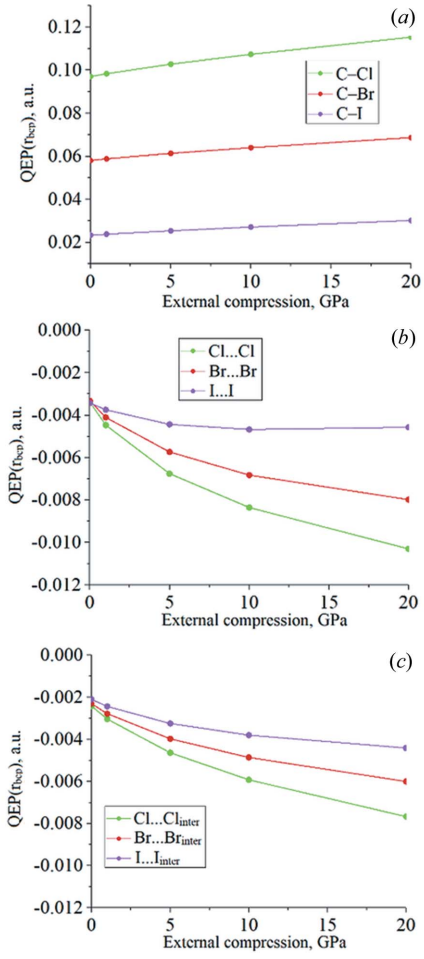

Figure 3
The change of quantum electronic pressure $\Delta QEP(\mathbf{r}_{bcp})$ for (*a*) C—Hal covalent bonds, (*b*) halogen bonds and (*c*) van der Waals stacking interactions under external compression.

3.1. Quantum electronic pressure distributions

The QEP(**r**) distributions obtained from the experimental (Fig. S1a) and calculated electron density (Fig. S1b), using the same expression (1), are nearly identical in the interatomic space of Cl_3-synthons: most of the isolines on the maps are reproduced very well. At bcp of the Cl···Cl halogen bonds and at rcp of Cl_3-synthons, the values of QEP(**r**) obtained from the different source electron density, both experimental (Bui *et al.*, 2009) and calculated in the present study, are also in good agreement (see Table S2). Thus, we have concluded that the theoretical quantum electronic pressure obtained by DFT calculations is worthy of further analysis.

Therefore, we consider QEP(**r**) to be a novel characteristic of changes in the crystalline continuum under external compression. Thus, we have modelled the distributions of QEP(**r**) in hexachlorobenzene (C_6Cl_6) hexabromobenzene (C_6Br_6) and hexaiodobenzene (C_6I_6) under external compression from 1 to 20 GPa. In general, the spatial QEP(**r**) 'inhomogeneity' in the intermolecular space of hexahalobenzene crystals is particularly pronounced. It mirrors different resistance to external stress of different regions such as the Hal···Hal stacking interactions or the halogen bonds. As a result, various structural fragments are responsible for different linear compressibility of the whole crystal. Fig. 2 illustrates the following features of QEP(**r**) distributions in the plane of Hal_3-synthons. Covalent bonds are characterized by QEP(**r**) > 0. It indicates the positive quantum contribution to the local internal energy of the electron continuum as a factor preventing compression of the covalent bonds. For Hal_3-synthons and Hal···Hal halogen bonds, QEP(**r**) is negative, *i.e.* the quantum contributions to the local internal energy compensates the growth of external compression of the elec-

tron continuum, which increases electron density as a result of shortening intermolecular distances in a crystal. Thus, the negative QEP(**r**) areas reveal the tendency of relative 'softness' for Hal···Hal halogen bonds and stacking interactions. In the C_6Cl_6 crystal [Fig. 2(*a*)], the less negative QEP(**r**) values form a peak at the centre of Cl_3-synthon. Under increasing external compression, the trough in the σ-hole regions diminish in size and deepen, also they can be distorted in shape. For C_6Br_6 the picture is not much different [Fig. 2(*b*)]; the separate region of the less negative values at the centre of a triangle formed by the Br···Br halogen bonds is hardly noticeable. The pattern of QEP(**r**) in the C_6I_6 crystal [Fig. 2(*c*)] is quite different. Under compression of 20 GPa, the trough near σ-holes are aligned along with decreasing negative QEP(**r**) values. It leads to nearly uniform distribution of QEP(**r**) in the whole I_3-synthon. Thus, QEP(**r**) in the I_3-synthon, in contrast to Cl_3- and Br_3-synthons, is characterized by the absence of pronounced peaks and troughs and by more uniform distribution of QEP(**r**).

As for the changes in quantum electronic pressure, ΔQEP($\mathbf{r}_{bcp}$), if the external pressure is increased to 20 GPa, we can compare the properties of the Hal···Hal noncovalent bonds in different crystals. For all Hal···Hal stacking interactions, halogen bonds and Hal_3-synthons, QEP($\mathbf{r}_{bcp}$) < 0 and QEP($\mathbf{r}_{rcp}$) < 0 [Figs. 3(*b*) and 3(*c*)]. Note that with a relatively uniform increase of electron density over the whole intermolecular space, the QEP($\mathbf{r}_{bcp}$) value for stacking interactions never exceeds the QEP($\mathbf{r}_{bcp}$) for the strongest halogen bond (in absolute value). This observation can be interpreted as follows: shortening a halogen bond leads to a greater gain in quantum contribution to internal energy than shortening the distances between the halogen atoms that occurs when the stacking volume decreases. This is in good agreement with the nature of all compared Hal···Hal noncovalent interactions. For an electrostatically-driven halogen bond, the Hal atoms with greater anisotropy in the valence electron shells are brought together easily, while the obstacles for convergence of electronegative electron lone-pair belts are quite obvious.

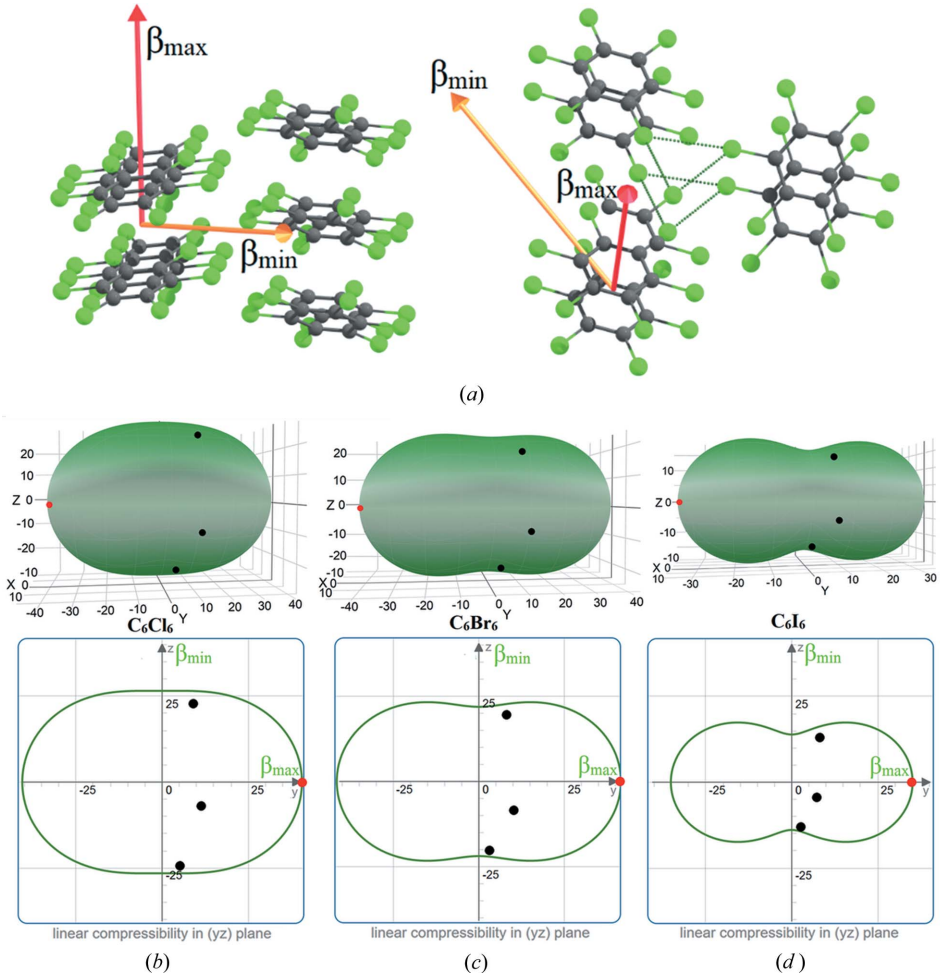

Figure 4
(*a*) Directions of maximal and minimal linear compressibility in the C_6Cl_6 crystal; the surfaces representing the spatial dependences of linear compressibility (top) and their 2D projections on the *yz* plane (bottom) for (*b*) C_6Cl_6, (*c*) C_6Br_6 and (*d*) C_6I_6 uncompressed crystals. Positions corresponding to the three Hal···Hal halogen bonds of Hal_3-synthon are depicted by black dots, the Hal···Hal stacking interactions are shown as the red dots.

Let us compare the trends of QEP($\mathbf{r}_{bcp}$) behaviour for the Hal···Hal interactions. The QEP($\mathbf{r}_{bcp}$) value changes more steeply for the halogen bonds than for the stacking interactions [Figs. 3(*b*) and 3(*c*)]. The largest changes under external compression up to 20 GPa have been observed in the C_6Cl_6 crystal; the relative ΔQEP($\mathbf{r}_{bcp}$) values comprise, on average, 256.6% for the Cl···Cl halogen bonds and 216.4% for the Cl···Cl stacking interactions. In the C_6Br_6 crystal relative lowering QEP($\mathbf{r}_{bcp}$) for the Br···Br halogen bonds (187.0%) slightly exceeds such lowering for stacking interactions (160.0%), meanwhile the I···I halogen bonds show the smallest value of ΔQEP($\mathbf{r}_{bcp}$), which is only 57.3% (Table 1).

3.2. Linear compressibility trends

The spatial dependency of linear compressibility is the set of its values forming a surface in three-dimensional space. To compare the orientation of specific bonds with the directions of maximal or minimal compressibility of a crystal, we can determine the coordinates of a point corresponding to the projection of bond direction on the surface. Any of these points corresponds to the value of linear compressibility in the direction along which the considered bond is elongated. Using the *ELATE* tools (Gaillac *et al.*, 2016; Gaillac & Coudert, 2016), we have compared the arrangements of the Hal···Hal halogen bonds and stacking interactions for all C_6Hal_6 crystals. The three black points on the surfaces in Figs. 4(*b*)–4(*d*) denote the projections corresponding to the three Hal···Hal halogen bonds of Hal_3-synthons. All three black points are located near the 'tight belt'. It means that all three Hal···Hal halogen bonds of the Hal_3-synthon are nearly perpendicular [Fig. 4(*a*)] to the direction of maximal linear compressibility, β_{max}, which has been determined from the spatial dependences of linear compressibility for the considered crystals. Note that the 'tightest belt' is observed for the C_6I_6 crystal.

We also considered the spatial dependences of linear compressibility as 2D projections in Cartesian coordinates. The *yz* plane of 2D projections for C_6Hal_6 crystals is the most informative [Figs. 4(*b*)–4(*d*)]. The disposition of the informative points in this plane guarantees that Hal···Hal interactions along the stacks of hexahalobenzene rings strictly coincide with the direction of maximal linear compressibility. The location of red points on the *y* axis indicates this fact. The values of linear compressibility are comparable for all C_6Hal_6 crystals; nevertheless, for C_6I_6, the contour of spatial dependences outlines noticeably smaller values along the *x* and *y* directions. Thus, the highest anisotropy of linear compressibility is observed for the C_6I_6 crystal.

Insofar as bulk modulus represents the directionally averaged linear compressibility, it can be recommended for characterization of relative crystal resistance to external hydrostatic compression. Calculated bulk moduli for the unstrained C_6Cl_6, C_6Br_6 and C_6I_6 crystals are 11.3, 12.2 and 17.3 GPa, respectively. The trends of calculated bulk moduli, B^E, obtained from stiffness tensor calculations in *ELATE* (Gaillac *et al.*, 2016; Gaillac & Coudert, 2016) and by the third-order Birch–Murnaghan equation in PASCal online tool (Cliffe & Goodwin, 2012), (Table S9) are in agreement with experimentally observed data (Vaidya & Kennedy, 1971; Nakayama *et al.*, 2000; Tateyama & Ohno, 2002). All calculated results show systematic overestimations, probably due to the fact that *ab initio* calculations have been carried out for 0 K ignoring the temperature effects. From the values of elastic moduli it follows that C_6I_6 is the most rigid and C_6Cl_6 is the most compliant of all considered crystals. It is in good agreement with the fact that the C_6Cl_6 crystal is soft. The possibility of plastic bending of this crystal was experimentally shown (Reddy *et al.*, 2006; Panda *et al.*, 2015). These observations are consistent with the trends in ΔQEP($\mathbf{r}_{bcp}$) behaviour for all types of Hal···Hal noncovalent bonds. In the C_6I_6 crystal the smallest changes in QEP($\mathbf{r}_{bcp}$) values are observed; in contrast in the C_6Cl_6 crystal both absolute and relative ΔQEP($\mathbf{r}_{bcp}$) values are the largest.

Under the simulated external pressure of 20 GPa, the strong decrease of linear compressibility is observed in all directions of considered crystals; this change is accompanied by the decrease in the anisotropy of elastic moduli. It corresponds to our observations that the decrease in linear compressibility along the Hal···Hal stacking interactions of hexahalobenzene rings, β_{max}, is always greater than the decrease in β_{min}, related to the deformation of Hal_3-synthons.

Thus, on the basis of the calculated linear compressibility and quantum electronic pressure for the halogen bonds, we have concluded that Hal_3-synthons, built from the 'soft' halogen bonds, create the 'stiff framework' in the hexahalobenzene crystals. The rigidity of Hal_3-synthons increases in the order $C_6Cl_6 < C_6Br_6 < C_6I_6$.

3.3. Quantum electronic pressure 'overfall' in Hal_3-synthons

For the centre of Hal_3-synthons in uncompressed crystals, the deepest negative value of QEP($\mathbf{r}_{rcp}$) is observed for I_3-synthon; for Cl_3-synthon, QEP($\mathbf{r}_{rcp}$) is closer to zero. Nevertheless, under increasing external compression, the QEP($\mathbf{r}_{rcp}$) values become more negative in series $C_6Cl_6 > C_6Br_6 > C_6I_6$; near the point of 5 GPa, the intersection of the trends 'QEP($\mathbf{r}_{rcp}$) *versus* external pressure' is observed for all Hal_3-synthons [Fig. 5(*a*)]. As a result, under 20 GPa the largest negative value of QEP($\mathbf{r}_{rcp}$) is in the C_6Cl_6 crystal, *i.e.* the sharpest QEP($\mathbf{r}_{rcp}$) change takes place in Cl_3-synthon. For the centres of benzene rings, the trends are not much different from each other, although the QEP($\mathbf{r}_{rcp}$) values vary. Thus, in the compressed C_6Cl_6, C_6Br_6 and C_6I_6 crystals the QEP($\mathbf{r}$) distributions inside Hal_3-synthons are significantly different from each other in comparison to Hal_3-synthons in the crystals under normal conditions.

It is interesting to compare the features of non-uniformity of electron continuum inside a Hal_3-synthon and its variations in the hexahalobenzene crystals. So we have analyzed the quantum electronic pressure 'overfall' in the plane of the Hal_3-synthon, *i.e.* Δ between QEP($\mathbf{r}_{rcp}$) at the centre of Hal_3-synthon and QEP($\mathbf{r}_{bcp}$) for the strongest halogen bond (ΔHal_3) (Table S10). Among the uncompressed crystals (0 GPa), the largest value of ΔHal_3 is observed in the C_6Cl_6

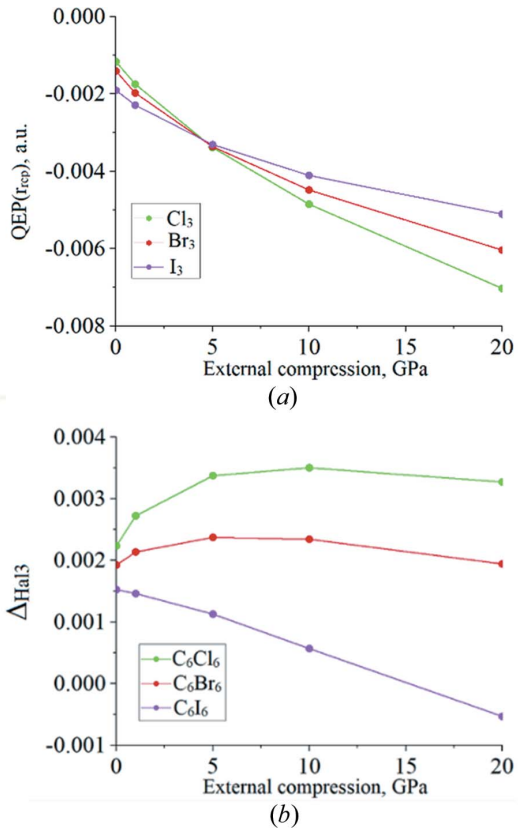

Figure 5
(*a*) The changes in quantum electronic pressure for Hal_3-synthon; (*b*) Δ of quantum electronic pressure between the centres of Hal_3-synthons and the strongest halogen bond.

crystal, and the smallest one is in C_6I_6 [Fig. 5(*b*)]. In the C_6Cl_6 and C_6Br_6 crystals, the quantum contribution to internal electronic energy, despite the halogen bonds shortening, is always higher than such a gain achieved at the centre of Hal_3-synthon. We can speculate that the rigidity of Cl_3-synthon is not provided only by the properties of the Cl···Cl halogen bonds. Its compressibility is held back by the QEP(**r**) at the centre of Cl_3-synthon. The maximum of ΔHal_3 is inherent for the hexahalobenzene crystals at different values of the external compression. In the C_6Cl_6 crystal, ΔCl_3 increases rapidly and reaches the maximum near 10 GPa. In Br_3-synthon, the change of ΔBr_3 is less pronounced, and the maximum of ΔBr_3 is observed closer to external pressure of 5 GPa. It is important to note, that in the C_6I_6 crystal the behaviour of QEP(**r**) is substantially distinct: ΔI_3 always decreases, and under 15–20 GPa, the absolute value of QEP($\mathbf{r}_{rcp}$) at the centre of I_3-synthon exceeds QEP($\mathbf{r}_{bcp}$) at the I···I halogen bond. It means that in the C_6I_6 crystal at the high external pressure the centre of I_3-synthon does not directly influence the resistance to external compression of such a fragment. The compression is held back by the properties of I···I noncovalent interactions, and such properties are detected by the function of quantum electronic pressure, QEP(**r**).

4. Conclusion

The mechanical stress distribution in the crystal under external hydrostatic pressure is nonuniform. Analysis of quantum electronic pressure, QEP(**r**), allows one to understand how the quantum effects reinforce the compressive strength for covalent bonds and how they counterbalance the growing stress for relatively 'soft' regions of intermolecular space. The negative quantum electronic pressure that is observed for halogen bonds and stacking interactions of halogen atoms locally decreases the internal stress caused by external compression when electron density increases.

The analysis of quantum electronic pressure under simulated hydrostatic compression was carried out for three isostructural organic crystals: hexachlorobenzene (C_6Cl_6), hexabromobenzene (C_6Br_6) and hexaiodobenzene (C_6I_6). The increase of electron density under the external compression from 0 to 20 GPa is approximately the same for all types of covalent and noncovalent bonds in all considered crystals. Nevertheless, the relative percentage of the electron density increase is two orders higher for noncovalent bonds than that for covalent bonds.

Under simulated external compression, the values of ΔQEP($\mathbf{r}_{bcp}$) show significant contrast for different types of bonds. For covalent bonds the positive QEP(**r**) values increase in order C—I < C—Br < C—Cl. Thus, the quantum effects maximize the stiffness of covalent bonds in the C_6Cl_6 crystal. For all noncovalent interactions the negative QEP(**r**) value decreases in order Cl···Cl > Br···Br > I···I, becoming even more negative when the external compression grows. This means that the quantum contribution reduces the local internal electronic energy in the intermolecular space to compensate the stress under the crystal deformation. The maximal relative change under compression is observed for the Cl···Cl halogen bond, meanwhile the I···I halogen bonds show the smallest value of ΔQEP($\mathbf{r}_{bcp}$). This is in good agreement with the calculated values of bulk moduli, increased in order C_6Cl_6 < C_6Br_6 < C_6I_6, and with experimentally observed plastic bending of the C_6Cl_6 crystal. Comparing the spatial QEP(**r**) 'non-uniformity' in Hal_3-synthons, we have observed that the behaviour of I_3-synthon is distinguished from that in the rest of crystals considered. The calculated linear compressibility of the crystals has convinced us that the 'softest' halogen bonds create the 'stiffest framework' in the hexahalobenzene crystals, if they are assembled in Hal_3-synthons. Finally, we note that quantum electronic pressure is a relevant and informative tool for characterization of the electron continuum features in molecular crystals and for observation of their anisotropy changing under external compression.

Funding information

Funding for this research was provided by: Russian Foundation for Basic Research (grant No. 20-03-00240); Ministry of Science and Higher Education of Russian Federation (grant No. 02.A03.21.0011, Act 211).

References

Aakeroy, C. B., Bryce, D. L., Desiraju, G. R., Frontera, A., Legon, A. C., Nicotra, F., Rissanen, K., Scheiner, S., Terraneo, G., Metrangolo, P. & Resnati, G. (2019). *Pure Appl. Chem.* **91**, 1889–1892.

Arkhipov, S. G., Losev, E. A., Nguyen, T. T., Rychkov, D. A. & Boldyreva, E. V. (2019). *Acta Cryst.* B**75**, 143–151.

Astakhov, A. A., Stash, A. I. & Tsirelson, V. G. (2016). *Int. J. Quantum Chem.* **116**, 237–246.

Bader, R. F. W. (1990). *Atoms in Molecules: A Quantum Theory*, pp. 1–438. Oxford: Clarendon Press.

Bader, R. F. W. (1991). *Chem. Rev.* **91**, 893–928.

Bag, P. P., Chen, M., Sun, C. C. & Reddy, C. M. (2012). *CrystEngComm*, **14**, 3865–3867.

Bartashevich, E. V. & Tsirelson, V. G. (2018). *J. Comput. Chem.* **39**, 573–580.

Bartashevich, E., Yushina, I., Kropotina, K., Muhitdinova, S. & Tsirelson, V. (2017). *Acta Cryst.* B**73**, 217–226.

Bartashevich, E. V., Yushina, I. D., Stash, A. I. & Tsirelson, V. G. (2014). *Cryst. Growth Des.* **14**, 5674–5684.

Becke, A. D. (1988). *Phys. Rev. A*, **38**, 3098–3100.

Bosch, E. & Barnes, C. L. (2002). *Cryst. Growth Des.* **2**, 299–302.

Brezgunova, M. E., Aubert, E., Dahaoui, S., Fertey, P., Lebègue, S., Jelsch, C., Ángyán, J. G. & Espinosa, E. (2012). *Cryst. Growth Des.* **12**, 5373–5386.

Bui, T. T. T., Dahaoui, S., Lecomte, C., Desiraju, G. R. & Espinosa, E. (2009). *Angew. Chem. Int. Ed.* **48**, 3838–3841.

Casati, N., Genoni, A., Meyer, B., Krawczuk, A. & Macchi, P. (2017). *Acta Cryst.* B**73**, 584–597.

Clark, T., Hennemann, M., Murray, J. S. & Politzer, P. (2007). *J. Mol. Model.* **13**, 291–296.

Cliffe, M. J. & Goodwin, A. L. (2012). *J. Appl. Cryst.* **45**, 1321–1329.

Colmenero, F. (2019*a*). *Phys. Chem. Chem. Phys.* **21**, 2673–2690.

Colmenero, F. (2019*b*). *Mater. Res. Expr.* **6**, 045610.

Coudert, F.-X. & Fuchs, A. H. (2016). *Coord. Chem. Rev.* **307**, 211–236.

Desiraju, G. R., Ho, P. S., Kloo, L., Legon, A. C., Marquardt, R., Metrangolo, P., Politzer, P., Resnati, G. & Rissanen, K. (2013). *Pure Appl. Chem.* **85**, 1711–1713.

Desiraju, G. R. & Parthasarathy, R. (1989). *J. Am. Chem. Soc.* **111**, 8725–8726.

Dovesi, R., Erba, A., Orlando, R., Zicovich-Wilson, C. M., Civalleri, B., Maschio, L., Rérat, M., Casassa, S., Baima, J., Salustro, S. & Kirtman, B. (2018). *WIREs Comput. Mol. Sci.* **8**, e1360.

Feng, G., Jiang, X., Wei, W., Gong, P., Kang, L., Li, Z., Li, Y., Li, X., Wu, X., Lin, Z., Li, W. & Lu, P. (2016). *Dalton Trans.* **45**, 4303–4308.

Feynman, R. P. (1939). *Phys. Rev.* **56**, 340–343.

Francl, M. M., Pietro, W. J., Hehre, W. J., Binkley, J. S., Gordon, M. S., DeFrees, D. J. & Pople, J. A. (1982). *J. Chem. Phys.* **77**, 3654–3665.

Gaillac, R. & Coudert, F.-X. (2016). *ELATE: Elastic Tensor Analysis*, http://progs.coudert.name/elate.

Gaillac, R., Pullumbi, P. & Coudert, F.-X. (2016). *J. Phys. Condens. Matter*, **28**, 275201.

Gatti, C. (1996). *Acta Cryst.* A**52**, C555–C556.

Gatti, C. & Casassa, S. (2016). *TOPOND14 User's Manual.* CNR-ISTM, Milan, Italy.

Ghosh, S., Reddy, C. M. & Desiraju, G. R. (2007). *Acta Cryst.* E**63**, o910–o911.

Giordano, N., Afanasjevs, S., Beavers, C. M., Hobday, C. L., Kamenev, K. V., O'Bannon, E. F., Ruiz-Fuertes, J., Teat, S. J., Valiente, R. & Parsons, S. (2019). *Molecules*, **24**, 2018.

Godbout, N., Salahub, D. R., Andzelm, J. & Wimmer, E. (1992). *Can. J. Chem.* **70**, 560–571.

Grimme, S., Antony, J., Ehrlich, S. & Krieg, H. (2010). *J. Chem. Phys.* **132**, 154104.

Groom, C. R., Bruno, I. J., Lightfoot, M. P. & Ward, S. C. (2016). *Acta Cryst.* B**72**, 171–179.

Hansen, N. K. & Coppens, P. (1978). *Acta Cryst.* A**34**, 909–921.

Hathwar, V. R. & Guru Row, T. N. (2010). *J. Phys. Chem. A*, **114**, 13434–13441.

Hunter, G. (1986). *Int. J. Quantum Chem.* **29**, 197–204.

Iwasaki, E., Shimizu, K., Amaya, K., Nakayama, A., Aoki, K. & Carlón, R. P. (2001). *Synth. Met.* **120**, 1003–1004.

Jetti, R. K. R., Xue, F., Mak, T. C. W. & Nangia, A. (1999). *Cryst. Eng.* **2**, 215–224.

Kirzhnits, D. A. (1957). *Sov. Phys. JETR*, **5**, 64–71.

Koch, W. & Holthausen, M. C. (2001). *In A Chemist's Guide to Density Functional Theory*, Wiley-VCH Verlag GmbH & Co. KGaA, Weinheim, Germany.

Kostenetskiy, P. & Semenikhina, P. (2018). *SUSU Supercomputer Resources for Industry and Fundamendal Science.* 2018 Global Smart Industry Conference (GloSIC), IEEE.

Lin, H., Chen, J.-F., Cui, Y.-M., Zhang, Z.-J., Yang, D.-D., Zhu, S.-G. & Li, H.-Z. (2017). *J. Energetic Mater.* **35**, 157–171.

Macchi, P. & Coppens, P. (2001). *Acta Cryst.* A**57**, 656–662.

Matveychuk, Y. V., Bartashevich, E. V. & Tsirelson, V. G. (2018). *Cryst. Growth Des.* **18**, 3366–3375.

Mishra, A. K., Murli, C., Pandey, K. K., Sakuntala, T., Poswal, H. K. & Verma, A. K. (2020). *J. Phys. Chem. B*, **124**, 373–379.

Mishra, M. K., Ghalsasi, P., Deo, M. N., Bhatt, H., Poswal, H. K., Ghosh, S. & Ganguly, S. (2017). *CrystEngComm*, **19**, 7083–7087.

Moussallem, C., Allain, M., Mallet, C., Gohier, F. & Frère, P. (2015). *J. Fluor. Chem.* **178**, 34–39.

Murray, J. S. & Politzer, P. (2011). *WIREs Comput. Mol. Sci.* **1**, 153–163.

Nakayama, A., Aoki, K. & Carlón, R. P. (2001). *Phys. Rev. B Condens. Matter*, **64**, 064104.

Nakayama, A., Fujihisa, H., Aoki, K. & Carlón, R. P. (2000). *Phys. Rev. B*, **62**, 8759–8765.

Panda, M. K., Ghosh, S., Yasuda, N., Moriwaki, T., Mukherjee, G. D., Reddy, C. M. & Naumov, P. (2015). *Nat. Chem.* **7**, 65–72.

Pavan, M. S., Durga Prasad, K. & Guru Row, T. N. (2013). *Chem. Commun.* **49**, 7558–7560.

Pavan, M. S. & Guru Row, T. N. (2016). *J. Chem. Sci.* **128**, 1579–1587.

Perdew, J. P., Burke, K. & Ernzerhof, M. (1996). *Phys. Rev. Lett.* **77**, 3865–3868.

Perger, W. F., Criswell, J., Civalleri, B. & Dovesi, R. (2009). *Comput. Phys. Commun.* **180**, 1753–1759.

Politzer, P. & Murray, J. S. (2019). *Crystals*, **9**, 165–179.

Pravica, M., Sneed, D., Wang, Y., Smith, Q. & White, M. (2016). *J. Phys. Chem. B*, **120**, 2854–2858.

Reddy, C. M., Kirchner, M. T., Gundakaram, R. C., Padmanabhan, K. A. & Desiraju, G. R. (2006). *Chem. Eur. J.* **12**, 2222–2234.

Rusek, M., Kwaśna, K., Budzianowski, A. & Katrusiak, A. (2020). *J. Phys. Chem. C*, **124**, 99–106.

Saha, B. K., Jetti, R. K. R., Reddy, L. S., Aitipamula, S. & Nangia, A. (2005). *Cryst. Growth Des.* **5**, 887–899.

Saha, S., Mishra, M. K., Reddy, C. M. & Desiraju, G. R. (2018). *Acc. Chem. Res.* **51**, 2957–2967.

Shirotani, I., Onodera, A., Kamura, Y., Inokuchi, H. & Kawai, N. (1976). *J. Solid State Chem.* **18**, 235–239.

Siram, R. B. K., Karothu, D. P., Guru Row, T. N. & Patil, S. (2013). *Cryst. Growth Des.* **13**, 1045–1049.

Stash, A. & Tsirelson, V. (2002). *J. Appl. Cryst.* **35**, 371–373.

Stash, A. I. & Tsirelson, V. G. (2005). *Crystallogr. Rep.* **50**, 177–184.

Stash, A. I. & Tsirelson, V. G. (2014). *J. Appl. Cryst.* **47**, 2086–2089.

Tao, J., Vignale, G. & Tokatly, I. V. (2008). *Phys. Rev. Lett.* **100**, 206405.

Tateyama, Y. & Ohno, T. (2002). *J. Phys. Condens. Matter*, **14**, 10429–10432.

Tsirelson, V. G. & Ozerov, R. P. (1996). *Electron Density and Bonding in Crystals.* Bristol, Philadelphia: IOP.
Tsirelson, V. G., Stash, A. I. & Tokatly, V. (2016). *Mol. Phys.* **114**, 1260–1269.
Tsirelson, V. G., Stash, A. I. & Tokatly, I. V. (2019). *Acta Cryst.* B**75**, 201–209.
Tsirelson, V. G., Zhou, P. F., Tang, T.-H. & Bader, R. F. W. (1995). *Acta Cryst.* A**51**, 143–153.
Vaidya, S. N. & Kennedy, G. C. (1971). *J. Chem. Phys.* **55**, 987–992.
Yang, Z.-Z. & Davidson, E. R. (1997). *Int. J. Quantum Chem.* **62**, 47–53.
Zhao, D.-X. & Yang, Z.-Z. (2014). *J. Phys. Chem. A*, **118**, 9045–9057.